CHAPTER 7

Approaching Control Based on a Tether Releasing Mechanism

The operation robot should arrive at the appointed position and keep its relative attitude stable before starting on-orbit service. The key technology for this procedure consists of optimal trajectory planning, tracking control, and relative attitude stability. Therefore in this chapter, a coordinated coupling control method for tracking the optimal trajectory is provided by utilizing a tether releasing mechanism, space tether, and thrusters.

It is necessary to select a proper method for establishing optimal trajectory planning model. An optimal trajectory planning problem is a kind of optimal control process that is under restricted conditions, such as path, control, or other constraints. The optimal index is fuel consumption or approach time. For an optimal trajectory planning problem, Ulybyshev presented a trajectory optimization method for low-thrust spacecraft proximity maneuvering at near-circular orbits, which used the discretization of a spacecraft trajectory on segments and sets of pseudoimpulses for each segment [1,2]. Suzuki presented a sequential goal programming approach, which considered not only well-defined flight trajectory problems but also ill-defined problems, and a fuzzy decision-making method was applied for the optimization that was not precisely prioritized in this method [3]. An interval optimization was proposed according to the fixed-time multiple impulse rendezvous and docking problem [4].

These methods represent the development of optimal control problems in recent years. However, they focus on long-distance optimal trajectory planning. In this chapter, the released tether is at the 200 m level. Therefore a universal trajectory planning method should be used for short distance situations. The pseudospectral method [5–7] is a popular direct method that parameterizes the state and control variables using orthogonal polynomials such as Legendre and Chebyschev polynomial. The use of global polynomials, together with the Gauss quadrate collocation points, is known to provide accurate approximations that converge exponentially for problems

Tethered Space Robot
https://doi.org/10.1016/B978-0-12-812309-6.00007-5

whose solutions are smooth [8]. This method is widely used for many trajectory optimization applications. Therefore it is appropriate to select this method to obtain the optimal approaching trajectory of the TSR.

For coordinated control using a tether, the collaborative control of tension (controlled by the service satellite), and thruster (controlled by a tethered robot) was investigated in approaching the target of the tethered retriever but it did not consider the attitude in Ref. [9]. Nohmi designed a tethered space robot, connected to a mother spacecraft through a tether. The tethered subsystem's attitude can be controlled by the tether tension through its link motion, and the tethered subsystem rotates when its mass center deviates from equilibrium, controlled by the arm [10]. They also developed a space robot attached to a spacecraft through a tether. The spacecraft-mounted manipulator generated the necessary initial momentum for the space robot and adjusted its trajectory by controlling the tether tension [11]. Mori proposed the concept of tethered satellite cluster systems whose parts were connected by tethers. He established the coordinated control method using tension and thrust, which decreased the fuel consumption of the thruster and improved control precision [12]. A coordinated fault-tolerant nonlinear control design was presented by Godard [13] to control the attitude of a satellite by using the movement of the tether attachment points; and his method examined cases when tether deployment suddenly stops and tether breakage occurs. However, these methods all focused on tether tension force where the tension force is applied to control input directly. It is difficult to impose the desired tension force. The releasing characteristics and construction of releasing mechanism are not considered. Therefore these coordinated methods are theoretical and ideal methods.

In this chapter, tension force input is replaced by the control torque of the motor, which can be easily imposed by the releasing motor. And the coordinated coupling position and attitude control law is designed by combining the releasing motor and thrusters of operation robot.

7.1 COUPLING DYNAMIC MODELS

7.1.1 Releasing Dynamic Model

First, the releasing dynamic model of the TSR is derived. The mass of the space tether is ignored, and the robot platform and operational robot are modeled as two point masses when we establish the orbital dynamic model

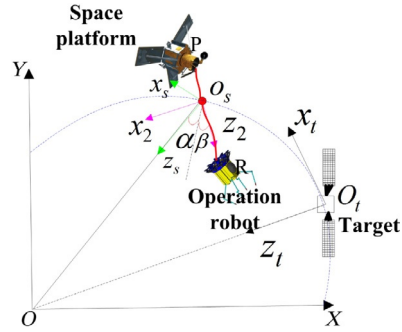

Fig. 7.1 Relevant coordinate frame of TSR.

of operational robot, which are represented as symbols R and P in a circular orbit. Define o_s as the centroid of the TSR, the $o_s x_s y_s z_s$ as the TSR orbit coordinate frame, and the $o_s x_2 y_2 z_2$ as the coordinate frame of space tether. The in-plane and out-of-plane angles are α and β. All the symbols are shown in Fig. 7.1.

Assume: $\boldsymbol{F}_P$ and $\boldsymbol{F}_R$ are the net forces acting on the space platform and operation robot, m_P and m_R denote the masses of two bodies respectively. $\mu = 3.986005 \times 10^{14}\ \mathrm{m}^3/\mathrm{s}^2$ is the earth gravitational constant. F_t is the tension force of space tether. $\boldsymbol{F} = [F_1, F_2, F_3]^{\mathrm{T}}$ is the thruster force of the operation robot in $o_s x_2 y_2 z_2$ coordinate frame. $\boldsymbol{r}_p$ and $\boldsymbol{r}_r$ are the position vectors from the O to the end-body P and R. $\boldsymbol{r}_{o_s}^p$ and $\boldsymbol{r}_{o_s}^r$ are the position vectors from the O_s to P and R. The following dynamics equation of the TSR is obtained by Newton's second law:

$$\frac{\boldsymbol{F}_p}{m_p} - \frac{\boldsymbol{F}_r}{m_r} = \boldsymbol{a}_p - \boldsymbol{a}_r = \boldsymbol{a}_p^r \tag{7.1}$$

where $\boldsymbol{a}_p$ is the acceleration of space platform in inertial coordinate frame $OXYZ$, $\boldsymbol{a}_r$ the acceleration of the operation robot in inertial coordinate frame $OXYZ$,and $\boldsymbol{a}_p^r$ the acceleration of space platform relative to the operation robot. $\boldsymbol{a}_p$ and $\boldsymbol{a}_r$ can be expressed by:

$$\boldsymbol{a}_p = -\frac{\mu}{|\boldsymbol{r}_p|^2}\frac{\boldsymbol{r}_p}{|\boldsymbol{r}_p|} + \frac{F_t}{m_p}\frac{\boldsymbol{r}_{o_s}^p}{|\boldsymbol{r}_{o_s}^p|} \tag{7.2}$$

$$\boldsymbol{a}_r = -\frac{\mu}{|\boldsymbol{r}_r|^2}\frac{\boldsymbol{r}_r}{|\boldsymbol{r}_r|} + \frac{F_t}{m_r}\frac{\boldsymbol{r}_{o_s}^r}{|\boldsymbol{r}_{o_s}^r|} + \frac{\boldsymbol{F}}{m_r} \tag{7.3}$$

The transformed matrix $\boldsymbol{C}_{o_s}^{l}$ from $o_s x_s y_s z_s$ to $o_s x_2 y_2 z_2$ can be obtained as follows:

$$\begin{aligned}\boldsymbol{C}_{o_s}^{l} &= \begin{bmatrix} 1 & 0 & 0 \\ 0 & \cos\beta & \sin\beta \\ 0 & -\sin\beta & \cos\beta \end{bmatrix} \begin{bmatrix} \cos\alpha & 0 & -\sin\alpha \\ 0 & 1 & 0 \\ \sin\alpha & 0 & \cos\alpha \end{bmatrix} \\ &= \begin{bmatrix} \cos\alpha & 0 & -\sin\alpha \\ \sin\alpha\sin\beta & \cos\beta & \cos\alpha\sin\beta \\ \sin\alpha\cos\beta & -\sin\beta & \cos\alpha\cos\beta \end{bmatrix}\end{aligned} \tag{7.4}$$

R_e is assumed to be the orbital radius, l the total releasing length of the space tether, l_R the tether length from R to o_s, l_P the tether length from P to o_s, and $\boldsymbol{r}_{o_s}$ the position vector of o_s in frame $OXYZ$. Therefore the position vector $\boldsymbol{r}_p$ and $\boldsymbol{r}_r$ can be expressed in the frame $o_s x_2 y_2 z_2$ as:

$$\boldsymbol{r}_p = \boldsymbol{r}_{o_s} + \boldsymbol{r}_p^{o_s} = \boldsymbol{C}_{o_s}^{l} \begin{bmatrix} 0 \\ 0 \\ -R_e \end{bmatrix} + \begin{bmatrix} 0 \\ 0 \\ -l_p \end{bmatrix} = \begin{bmatrix} R_e\sin\alpha \\ -R_e\cos\alpha\sin\beta \\ -R_e\cos\alpha\cos\beta - l_p \end{bmatrix} \tag{7.5}$$

$$\boldsymbol{r}_r = \boldsymbol{r}_{o_s} + \boldsymbol{r}_r^{o_s} = \boldsymbol{C}_{o_s}^{l} \begin{bmatrix} 0 \\ 0 \\ -R_e \end{bmatrix} + \begin{bmatrix} 0 \\ 0 \\ l_r \end{bmatrix} = \begin{bmatrix} R_e\sin\alpha \\ -R_e\cos\alpha\sin\beta \\ -R_e\cos\alpha\cos\beta + l_r \end{bmatrix} \tag{7.6}$$

In Eqs. (7.5) and (7.6), $\boldsymbol{r}_p^{o_s} = -\boldsymbol{r}_{o_s}^{p}$, $\boldsymbol{r}_r^{o_s} = -\boldsymbol{r}_{o_s}^{r}$. The following equations are easily obtained:

$$\left|\boldsymbol{r}_p\right|^{-3} \approx \frac{1}{{R_e}^3}\left(1 - 3\frac{l_p}{R_e}\cos\alpha\cos\beta\right) \tag{7.7}$$

$$\left|\boldsymbol{r}_r\right|^{-3} \approx \frac{1}{{R_e}^3}\left(1 + 3\frac{l_r}{R_e}\cos\alpha\cos\beta\right) \tag{7.8}$$

Substitute Eqs. (7.2), (7.3), (7.5)–(7.8) into (7.1), and simplify, we have:

$$\frac{\boldsymbol{F}_p}{m_p} - \frac{\boldsymbol{F}_r}{m_r} = \begin{bmatrix} 3\Omega_r^2 l\sin\alpha\cos\alpha\cos\beta - \dfrac{F_1}{m_r} \\ -3\Omega_r^2 l\sin\beta\cos\beta\cos^2\alpha - \dfrac{F_2}{m_r} \\ -3\Omega_r^2 l\cos^2\alpha\cos^2\beta + \Omega_r^2 l + \dfrac{F_t}{\overline{m}} - \dfrac{F_3}{m_r} \end{bmatrix} \tag{7.9}$$

where $\overline{m} = \dfrac{m_p + m_r}{m_p m_r}$, $\Omega_r = \sqrt{\mu / R_e^3}$.

The relative angular velocity $\boldsymbol{\omega}_l^e$ and angular acceleration $\boldsymbol{\alpha}_l^e$ between the inertial frame $OXYZ$ and the frame $o_s x_2 y_2 z_2$ can be expressed in the frame $o_s x_2 y_2 z_2$ as:

$$\boldsymbol{\omega}_l^e = \begin{bmatrix} \dot{\beta} \\ (\dot{\alpha} - \Omega_r)\cos\beta \\ (-\dot{\alpha} + \Omega_r)\sin\beta \end{bmatrix}, \quad \boldsymbol{\alpha}_l^e = \begin{bmatrix} \ddot{\beta} \\ \ddot{\alpha}\cos\beta - (\dot{\alpha} - \Omega_r)\sin\beta\dot{\beta} \\ -\ddot{\alpha}\sin\beta - (\dot{\alpha} - \Omega_r)\cos\beta\dot{\beta} \end{bmatrix} \tag{7.10}$$

The ${}^l\boldsymbol{r}_p^r$ is the position vector from R to P, and its derivatives differentiated in the $o_s x_2 y_2 z_2$ frame, which can be expressed as:

$${}^l\boldsymbol{r}_p^r = \begin{bmatrix} 0 \\ 0 \\ -l \end{bmatrix}, \quad {}^l\boldsymbol{v}_p^r = \begin{bmatrix} 0 \\ 0 \\ -\dot{l} \end{bmatrix}, \quad {}^l\boldsymbol{a}_p^r = \begin{bmatrix} 0 \\ 0 \\ -\ddot{l} \end{bmatrix} \tag{7.11}$$

Define $\boldsymbol{n} = [n_x \;\; n_y \;\; n_z]^{\mathrm{T}}$ and $\boldsymbol{n}^{\times} = \begin{bmatrix} 0 & -n_z & n_y \\ n_z & 0 & -n_x \\ -n_y & n_x & 0 \end{bmatrix}$. The inertial acceleration $\boldsymbol{a}_p^r$ can be expressed as:

$$\boldsymbol{a}_p^r = {}^l\boldsymbol{a}_p^r + \boldsymbol{\alpha}_p^{r\times l}\boldsymbol{r}_p^r + 2\boldsymbol{\omega}_p^{r\times l}\boldsymbol{v}_p^r + \boldsymbol{\omega}_p^{r\times}\left(\boldsymbol{\omega}_p^{r\times l}\boldsymbol{r}_p^r\right) \tag{7.12}$$

Substitute Eqs. (7.10) and (7.11) into (7.12), simplify:

$$\boldsymbol{a}_p^r = \begin{bmatrix} -\ddot{\alpha}\cos\beta l + 2(\dot{\alpha} - \Omega_r)\sin\beta\dot{\beta}l - 2\dot{l}(\dot{\alpha} - \Omega_r)\cos\beta \\ l\ddot{\beta} + 2\dot{\beta}\dot{l} + (\dot{\alpha} - \Omega_r)^2\sin\beta\cos\beta l \\ -\ddot{l} + (\dot{\alpha} - \Omega_r)^2\cos^2\beta l + l\dot{\beta}^2 \end{bmatrix} \tag{7.13}$$

Substitute Eqs. (7.9) and (7.13) into (7.1), the releasing dynamic model of the TSR is given as:

$$\ddot{\alpha} + 2(\dot{\alpha} - \Omega_r)\left(\frac{\dot{l}}{l} - \dot{\beta}\tan\beta\right) + 3\Omega_r^2\sin\alpha\cos\alpha = \frac{1}{\cos\beta l}\frac{F_1}{m_r} \tag{7.14}$$

$$\ddot{\beta} + 2\frac{\dot{l}}{l}\dot{\beta} + \left[(\dot{\alpha} - \Omega_r)^2 + 3\Omega_r^2\cos^2\alpha\right]\sin\beta\cos\beta = -\frac{1}{l}\frac{F_2}{m_r} \tag{7.15}$$

$$\ddot{l} - l\cos^2\beta\left[(\dot{\alpha} - \Omega_r)^2 + 3\Omega_r^2\cos^2\alpha\right] + l\left(\Omega_r^2 - \dot{\beta}^2\right) = -\frac{F_t}{\overline{m}} + \frac{F_3}{m_r} \tag{7.16}$$

7.1.2 Attitude Dynamic Model

Assume: The body coordinate frame of the operation robot is $o_c x_c y_c z_c$. The attitude of the operation robot are expressed by ϕ_l, θ_l, and ψ_l, which are defined relative to tether coordinate frame $o_s x_2 y_2 z_2$.

$\boldsymbol{H}$ is assumed to be the angular momentum, $\boldsymbol{M}$ the external torques, which include control torque and disturbed torque. The following equation is obtained by momentum theorem:

$$\boldsymbol{M} = \frac{d\boldsymbol{H}}{dt} = \dot{\boldsymbol{H}} + \boldsymbol{\omega}^{\times}\boldsymbol{H} \tag{7.17}$$

where $\boldsymbol{\omega}$ is angular velocity of operation robot. Eq. (7.17) can be rewritten as:

$$\begin{bmatrix} M_x \\ M_y \\ M_z \end{bmatrix} = \begin{bmatrix} \dot{h}_x \\ \dot{h}_y \\ \dot{h}_z \end{bmatrix} + \begin{bmatrix} 0 & -\omega_z & \omega_y \\ \omega_z & 0 & -\omega_x \\ -\omega_y & \omega_x & 0 \end{bmatrix} \begin{bmatrix} h_x \\ h_y \\ h_z \end{bmatrix} \tag{7.18}$$

where $\boldsymbol{M}=[M_x \;\; M_y \;\; M_z]$, $\boldsymbol{H}=[h_x \;\; h_y \;\; h_z]$. And the angular momentum $\boldsymbol{H}$ can be expressed as:

$$h_x = I_x\omega_x - I_{xy}\omega_y - I_{xz}\omega_z \tag{7.19}$$

$$h_y = -I_{xy}\omega_x + I_y\omega_y - I_{yz}\omega_z \tag{7.20}$$

$$h_z = -I_{xz}\omega_x - I_{yz}\omega_y + I_z\omega_z \tag{7.21}$$

where $\boldsymbol{I}=\begin{bmatrix} I_x & -I_{xy} & -I_{xz} \\ -I_{xy} & I_y & -I_{yz} \\ -I_{xz} & -I_{yz} & I_z \end{bmatrix}$ is the inertia matrix, which can be calculated by:

$$I_x = \int_0^{m_r} \left(y^2 + z^2\right) dm \quad I_y = \int_0^{m_r} \left(x^2 + z^2\right) dm \quad I_z = \int_0^{m_r} \left(y^2 + x^2\right) dm \tag{7.22}$$

$$I_{xy} = \int_0^{m_r} (xy)\, dm \quad I_{yz} = \int_0^{m_r} (yz)\, dm \quad I_{xz} = \int_0^{m_r} (xz)\, dm \tag{7.23}$$

If the axes $o_c x_c$, $o_c y_c$, and $o_c z_c$ are defined as primary inertial axes, the following equation is obtained:

$$I_{xy} = 0, \quad I_{xz} = 0, \quad I_{yz} = 0 \tag{7.24}$$

Substituting Eqs. (7.19)–(7.21) and (7.24) into (7.17) and simplifying yield:

$$\begin{cases} M_x = I_x\dot{\omega}_x + \omega_y\omega_z\left(I_z - I_y\right) \\ M_y = I_y\dot{\omega}_y + \omega_x\omega_z\left(I_x - I_z\right) \\ M_z = I_z\dot{\omega}_z + \omega_x\omega_y\left(I_y - I_x\right) \end{cases} \tag{7.25}$$

According to the complex kinematics relationship of the operation robot, the angular velocity $\boldsymbol{\omega}$ is the sum of $\boldsymbol{\omega}_l^r$ and $\boldsymbol{\omega}_l$, which are described as:

$$\boldsymbol{\omega}_l^r = \begin{bmatrix} \dot{\phi}_l \\ \dot{\theta}_l \\ \dot{\psi}_l \end{bmatrix}, \quad \boldsymbol{\omega}_l = \begin{bmatrix} \cos\alpha & 0 & -\sin\alpha \\ \sin\alpha\sin\beta & \cos\beta & \cos\alpha\sin\beta \\ \sin\alpha\cos\beta & -\sin\beta & \cos\alpha\cos\beta \end{bmatrix} \begin{bmatrix} 0 \\ -\Omega_r \\ 0 \end{bmatrix} \tag{7.26}$$

$\boldsymbol{\omega}$ can be given as:

$$\boldsymbol{\omega} = \boldsymbol{\omega}_l^r + \begin{bmatrix} 1 & \psi_l & -\theta_l \\ -\psi_l & 1 & \phi_l \\ \theta_l & -\phi_l & 1 \end{bmatrix}, \quad \boldsymbol{\omega}_l = \begin{bmatrix} \dot{\phi}_l - \Omega_r\psi_l\cos\beta - \Omega_r\theta_l\sin\beta \\ \dot{\theta}_l - \Omega_r\cos\beta + \Omega_r\phi_l\sin\beta \\ \dot{\psi}_l + \Omega_r\phi_l\cos\beta + \Omega_r\sin\beta \end{bmatrix} \tag{7.27}$$

Assume $|\phi_l| \ll 1$ rad, $|\theta_l| \ll 1$ rad, and $|\psi_l| \ll 1$ rad. Substitute Eq. (7.27) into (7.25) and simplify, we have:

$$\begin{aligned} &\ddot{\phi}_l - n_x\Omega_r^2\left(\sin^2\beta - \cos^2\beta\right)\phi_l - (n_x+1)\Omega_r\sin\beta\dot{\theta}_l + (n_x-1)\Omega_r\cos\beta\dot{\psi}_l \\ &-\Omega_r\cos\beta\dot{\beta}\dot{\theta}_l + \Omega_r\sin\beta\dot{\beta}\psi_l + n_x\Omega_r^2\sin\beta\cos\beta = \frac{M_x}{I_x} \end{aligned} \tag{7.28}$$

$$\begin{aligned} &\ddot{\theta}_l - n_y\Omega_r\sin\beta\theta_l + \left(\sin\beta - n_y\sin\beta\right)\Omega_r\dot{\phi}_l + \Omega_r\cos\beta\dot{\beta}\phi_l \\ &-n_y\Omega_r^2\sin\beta\cos\beta\psi_l + \Omega_r\sin\beta\dot{\beta} = \frac{M_y}{I_y} \end{aligned} \tag{7.29}$$

$$\begin{aligned} &\ddot{\psi}_l + n_z\Omega_r^2\cos^2\beta\psi_l + (1-n_z)\Omega_r\cos\beta\dot{\phi}_l - \Omega_r\sin\beta\dot{\beta}\phi_l \\ &+ n_z\Omega_r^2\sin\beta\cos\beta\theta_l + \Omega_r\cos\beta\dot{\beta} = \frac{M_z}{I_z} \end{aligned} \tag{7.30}$$

where $n_x = \left(I_y - I_z\right)/I_x$, $n_y = \left(I_x - I_z\right)/I_y$, and $n_z = \left(I_y - I_x\right)/I_z$.

7.1.3 Model of Tether Releasing Mechanism

Firstly, the investigation of releasing mechanism of the space tether will be introduced in this section. For the research of tether releasing mechanism, the YES2 project designed one kind of tether reel mechanism, which can achieve control of a 30 km length tether for releasing or retrieving [14,15]. SEDS project designed one kind of releasing mechanism, which includes a motor, one reel, a tension sensor, and a shear cutter. This mechanism has already been used in some relative experiments of microgravity environment [16]. The Japanese Space Research Centre developed a

releasing reel mechanism [17,18], which consists of a reel, a brake motor, an optical encoder, and its control unit. Tether length and tension are not measured directly but calculated from the revolution of the reel instead when the tether is released from this mechanism. All of these releasing mechanisms have one common feature: the space tether can be stored in the reel, and tether can be released from the reel through driving the motor. The mechanism of "reel, motor" is one kind of useful control device. Therefore a simplified mechanism of "reel, motor" is adopted in this chapter, which is shown in Fig. 7.2.

Assume: The tension force of the space tether is F_t. The cross-section of the tether is A. The Yang's modulus is E. The rotating angle of the reel is ϕ_r. The releasing length of the tether is l_r, and the actual length of the tether is l. The damping coefficients of the tether and reel are C_t and C_d. The reel moment of inertia is I_r. The friction torque of the reel is T_l. The control torque of the motor is T_m. The reel width is w_d. The diameter of the space tether is d. The diameter of the reel is D_1 when the tether is not stored in the

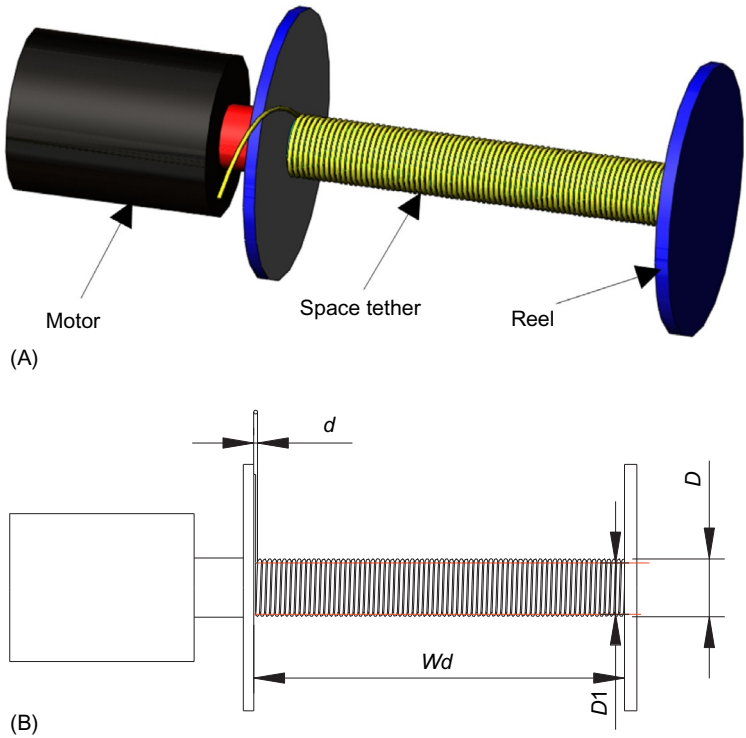

Fig. 7.2 The releasing mechanism of the space tether. (A) The construction of mechanism and (B) relative definition of mechanism.

reel, and the diameter of reel is D when the tether is totally stored in the reel, which is shown in Fig. 7.2B. According these assumptions, the tension force of the tether is calculated as following:

$$F_t = \frac{EA}{l_r}(l - l_r) + \frac{C_t EA}{l_r}(\dot{l} - \dot{l}_r) \tag{7.31}$$

If there are n layers of tether rolled in the reel, the D can be calculated by:

$$D = D_1 + 2nd \tag{7.32}$$

There are two methods for storing the tether in the reel, including the slack and tight arrangements. The coefficient γ $(0 < \gamma \leq 1)$ defines the different forms. If the coefficient satisfies the condition $\gamma = 1$, the space tether is stored tightly in the reel. Otherwise, it is stored slackly in the reel. It is defined that $r_d = d/2$, $r_1 = D_1/2$, and $r = D/2$. The tether volume is constant. Therefore the following equation is obtained.

$$\gamma w_d \pi\left(r^2 - r_1^2\right) = \pi(L_r - l_r)r_d^2 \tag{7.33}$$

where the L_r denotes the total length of the tether (releasing length and stored length).

In this chapter, assume $\gamma = 1$. Therefore Eq. (7.33) can be rewritten as:

$$w_d \pi\left(r^2 - r_1^2\right) = \pi(L_r - l_r)r_d^2 \tag{7.34}$$

The reel radius r can be calculated with the following equation.

$$r = \sqrt{S_2 - S_1 l_r} \tag{7.35}$$

where $S_1 = \dfrac{r_d^2}{\gamma w_d}$, $S_2 = S_1 L_r + r_1^2$.

Eq. (7.36) can be obtained by analyzing the construction and rotating law of the reel.

$$r\frac{d\phi_r}{dt} = \frac{dl_r}{dt} \tag{7.36}$$

Substitute Eq. (7.35) into (7.36), simplify:

$$\frac{d\phi_r}{dt} = \frac{1}{\sqrt{S_2 - S_1 l_r}}\frac{dl_r}{dt} \tag{7.37}$$

Integrated both sides of Eq. (7.37), Eq. (7.38) can be obtained.

$$\phi_r = -\frac{2}{S_1}\sqrt{S_2 - S_1 l_r} + C \tag{7.38}$$

where C is the integral constant. If we substitute $\phi_r(0)=0$, $l_r(0)=0$ into Eq. (7.38), C can be calculated:

$$C=\frac{2\sqrt{S_2}}{S_1} \tag{7.39}$$

Substituting Eq. (7.39) into (7.38), the following equation is obtained:

$$\phi_r=-\frac{2}{S_1}\sqrt{S_2-S_1 l_r}+\frac{2\sqrt{S_2}}{S_1} \tag{7.40}$$

The construction characteristic of the tether releasing mechanism is described in Eq. (7.40). According to the rotating law of the reel, we can easily obtain the dynamics model of the tether releasing mechanism.

$$I_r\ddot{\phi}_r+C_d\dot{\phi}_r=F_t r-T_l-T_m \tag{7.41}$$

The control torque of the motor is T_m, and the T_l is the friction torque between the tether and reel. The $F_t r$ is the disturbed torque of the space tether. The T_m can be defined as one control input, which can control the releasing length of space tether with the help of initial velocity.

7.1.4 Entire Coupled Dynamics Model

The releasing dynamics model, attitude dynamics of the TSR, and the construction dynamics of the releasing mechanism have been derived in the previous section. In this section, the 6-DOF coupled dynamics model of the TSR can be concluded based on these models.

Firstly, one condition should be proposed. The operation robot has initial velocity, also, the control torque of the motor can control the tether length with the help of initial velocity. The in-plane and out-of-plane angles can be controlled by the thrusters of the operation robot.

The releasing acceleration of $o_s z_2$ direction is designed by u_3. The thruster control force of $o_s x_2$ direction is u_1, and the thruster control force of $o_s y_2$ direction is u_2. The attitude control vector is $\boldsymbol{M_s}=[M_x \;\; M_y \;\; M_z]^{\mathrm{T}}$. Define the control torque of motor as T_m and the 6-DOF coupled dynamics model of the TSR are given as:

$$\ddot{\alpha}+2(\dot{\alpha}-\Omega_r)\left(\frac{\dot{l}}{l}-\dot{\beta}\tan\beta\right)+3\Omega_r^2\sin\alpha\cos\alpha=\frac{1}{\cos\beta l}\frac{u_1}{m_r} \tag{7.42}$$

$$\ddot{\beta}+2\frac{\dot{l}}{l}\dot{\beta}+\left[(\dot{\alpha}-\Omega_r)^2+3\Omega_r^2\cos^2\alpha\right]\sin\beta\cos\beta=-\frac{1}{l}\frac{u_2}{m_r} \tag{7.43}$$

$$\ddot{l} = u_3 \tag{7.44}$$

$$I_r\ddot{\phi}_r + C_d\dot{\phi}_r - F_t r + T_l = -T_m \tag{7.45}$$

$$\begin{aligned}&\ddot{\phi}_l - n_x\Omega_r^2\left(\sin^2\beta - \cos^2\beta\right)\phi_l - (n_x+1)\Omega_r\sin\beta\dot{\theta}_l + (n_x-1)\Omega_r\cos\beta\dot{\psi}_l \\ &-\Omega_r\cos\beta\dot{\beta}\dot{\theta}_l + \Omega_r\sin\beta\dot{\beta}\dot{\psi}_l + n_x\Omega_r^2\sin\beta\cos\beta = \frac{M_x}{I_x}\end{aligned} \tag{7.46}$$

$$\begin{aligned}&\ddot{\theta}_l - n_y\Omega_r\sin\beta\theta_l + \left(\sin\beta - n_y\sin\beta\right)\Omega_r\dot{\phi}_l + \Omega_r\cos\beta\dot{\beta}\phi_l \\ &-n_y\Omega_r^2\sin\beta\cos\beta\psi_l + \Omega_r\sin\beta\dot{\beta} = \frac{M_y}{I_y}\end{aligned} \tag{7.47}$$

$$\begin{aligned}&\ddot{\psi}_l + n_z\Omega_r^2\cos^2\beta\psi_l + (1-n_z)\Omega_r\cos\beta\dot{\phi}_l - \Omega_r\sin\beta\dot{\beta}\phi_l \\ &+ n_z\Omega_r^2\sin\beta\cos\beta\theta_l + \Omega_r\cos\beta\dot{\beta} = \frac{M_z}{I_z}\end{aligned} \tag{7.48}$$

7.2 COORDINATED COUPLING CONTROL STRATEGY

The tension force is treated as the control input, which is the common method of coordinated control. Generating the desired tension force of the space tether is not an easy task. Therefore this chapter proposed one coordinated control method with the consideration of the releasing characteristics. Compared with the previous coordinated control method, it is easy to understand the engineering application. The control torque of the releasing motor is treated as one control input, which can control the releasing length of the tether. However, the operation robot should have the initial velocity. Therefore the common tension force control is transformed into releasing motor control. In this chapter, the position tracking of three directions and the three axis attitude control are realized with the help of six thrusters of double directions and one releasing motor. First, the optimal approaching trajectory planning method is provided.

7.2.1 The Optimal Trajectory Planning

The dynamics model is shown as Eqs. (7.42)–(7.44) in the process of the optimal trajectory planning. Therefore the vectors u_1, u_2, and u_3 can be regarded as planning vectors. With state variables denoted by $\boldsymbol{X} = \left[\alpha, \beta, l, \dot{\alpha}, \dot{\beta}, \dot{l}\right]^{\mathrm{T}}$, the control force can be written by $\boldsymbol{u} = [u_1, u_2, u_3]^{\mathrm{T}}$. Therefore the dynamics model can be expressed by:

$$\dot{\boldsymbol{X}} = \boldsymbol{f}(\boldsymbol{X}, \boldsymbol{u}, t) \tag{7.49}$$

where $\boldsymbol{f}$ is a function among derivatives of the state variables, control variables, and time; as described by Eqs. (7.42)–(7.44); the control constraints must be enforced because the thrusters produce a control force that is bound by $F_{\max}$ and the tether acceleration is bound by a_{tmax}. The control constraints are limited as:

$$\begin{aligned} -F_{\max} \le u_1 \le F_{\max} \\ -F_{\max} \le u_2 \le F_{\max} \\ -a_{\text{t}}\max \le u_3 \le 0 \end{aligned} \tag{7.50}$$

The u_3 is negative, which is shown in Eq. (7.50). The tether can only supply a pulling force, however, it cannot provide pushing force.

It is assumed that $\boldsymbol{X}_0$ are the initial states, and $\boldsymbol{X}_f$ are the terminal states of the operation robot. The optimal trajectory should satisfy the appointed terminal constraints, which are represented by Eq. (7.51). In this chapter, the operation robot should arrive the terminal point, which must match the position and velocity relative to the target at the arrival time t_f, which can be expressed by the form:

$$\boldsymbol{\Phi}\left(\boldsymbol{X}_0, \boldsymbol{X}_f\left(t_f\right)\right) = 0 \tag{7.51}$$

where $\boldsymbol{\Phi}$ is the function of terminal constraint. The thruster fuel of operation robot is limited in the process of approaching the target. Therefore minimal fuel consumption is preferential, and the approach time t_f is not optimized. The trajectory optimization performance index J_g is written as:

$$J_g = \int_{t_0}^{t_f} \boldsymbol{u_g}^{\text{T}}(t)\boldsymbol{u_g}(t)dt \tag{7.52}$$

Where $\boldsymbol{u_g} = [u_1, u_2]^{\text{T}}$. The states of the operation robot should be restricted. Therefore the path constraints are expressed as follows:

$$\boldsymbol{X}_{\min} \le \boldsymbol{X} \le \boldsymbol{X}_{\max} \tag{7.53}$$

where $\boldsymbol{X}_{\min}$ and $\boldsymbol{X}_{\max}$ are the minimum and maximum of the state variables separately.

Thus the basic task is now to design an optimal trajectory that satisfies the differential constraints in Eq. (7.49), control constraints in Eq. (7.50), initial conditions $\boldsymbol{X}_0$, terminal constrains in Eq. (7.51), path constraints in Eq. (7.53), and at the same time making the performance index in Eq. (7.52) as small as possible.

The optimal approaching trajectory of the operation robot is design by a pseudospectral method now. The pseudospectral method in the trajectory

optimization is a special scheme, which transcribes a continuous dynamic optimization problem to a nonlinear programming (NLP) problem. Among the various orthogonal polynomials utilized by the pseudospectral method, which are all defined in the normalized domain $[-1,1]$. First, time domain is transformed by introducing the following equation:

$$\tau = \frac{2t}{t_f - t_0} - \frac{t_f + t_0}{t_f - t_0} \tag{7.54}$$

where $\tau \in [-1,1]$ is the normalized time. Thus the dynamics of operation robot in Eq. (7.49) can be transformed into:

$$\frac{d}{d\tau}\boldsymbol{X} = \frac{t_f - t_0}{2}\boldsymbol{f}(\boldsymbol{X}, \boldsymbol{u}, \tau) \tag{7.55}$$

It can approximate the state variables $\boldsymbol{X}$ by Lagrange interpolation. Then, the state variables $\boldsymbol{X}$ can be written as:

$$\boldsymbol{X}(\tau) = \sum_{i=0}^{M} L_i(\tau)\boldsymbol{X}(\tau_i) \tag{7.56}$$

where $L_i(\tau) = \prod_{j=0, j\neq i}^{M} \frac{\tau - \tau_j}{\tau_i - \tau_j}$ is the Lagrange interpolation polynomial based on the Legendre-Gauss (LG) point τ_h, $h = 1, 2 \ldots M$, and point $\tau_0 = -1$ is appended by the Gauss pseudospectral method. And the LG point τ_h are the roots of:

$$P_M(\tau) = \frac{1}{2^M M!}\frac{d^M}{d\tau^M}\left[\left(\tau^2 - 1\right)^M\right] = 0 \tag{7.57}$$

However, the state variables $\boldsymbol{X}(\tau)$ do not contain the discrete point at operation time $\tau_f = 1$. Thus the final variable can be discretized and approximated via the Gauss quadrature.

$$\boldsymbol{X}(\tau_f) - \boldsymbol{X}(\tau_0) - \frac{t_f - t_0}{2}\sum_{i=1}^{M} \omega_i \boldsymbol{f}\left(\boldsymbol{X}(\tau_i), \boldsymbol{U}(\tau_i), \tau_i; t_0, t_f\right) = 0 \tag{7.58}$$

where $\omega_i = \frac{2}{(1-\tau_i^2)\left[\dot{P}_M(\tau_i)\right]^2}$, $i = 1, 2, \ldots, M$ are the Gauss weights, $\boldsymbol{U}(\tau_i)$ are approximation of discrete control force. The control variables $\boldsymbol{u}$ are then approximated by Lagrange interpolation:

$$\boldsymbol{u}(\tau) = \sum_{i=1}^{M} \widetilde{L}_i(\tau)\boldsymbol{U}(\tau_i) \tag{7.59}$$

where $\widetilde{L}_i(\tau) = \prod_{j=1, j\neq i}^{M} \frac{\tau - \tau_j}{\tau_i - \tau_j}$ is the Lagrange interpolation polynomial based on LG point τ_h, $h = 1, 2, \ldots, M$.

The derivatives of the state variables $\boldsymbol{X}(\tau)$ are estimated by differentiating Eq. (7.56).

$$\frac{d\boldsymbol{X}(\tau_k)}{d\tau} = \sum_{i=0}^{M} \dot{L}_i(\tau_k)\boldsymbol{X}(\tau_i) = \sum_{i=0}^{M} D_{ki}\boldsymbol{X}(\tau_i), \quad (k = 1, 2, \ldots, M) \tag{7.60}$$

where

$$D_{ki} = \dot{L}_i(\tau_k) = \sum_{l=0}^{M} \frac{\prod_{j=0, j\neq i, l}^{M} (\tau_k - \tau_j)}{\prod_{j=0, j\neq i}^{M} (\tau_i - \tau_j)}$$

which are the element of the $M \times (M+1)$ differentiation matrix $\boldsymbol{D}$.

The dynamics of the TSR can be approximated by imposing it at some specific nodes. At these nodes, the following equations are satisfied:

$$\boldsymbol{R}_k = \sum_{i=0}^{M} D_{ki}\boldsymbol{X}_i - \frac{t_f - t_0}{2} f\left(\boldsymbol{X}_k, \boldsymbol{U}_k, \tau_k; t_0, t_f\right) = 0, \quad (k = 1, \ldots, M) \tag{7.61}$$

Thus the algebraic constrains are imposed by the LG point τ_k, $k = 1, 2, \ldots, M$. And the boundary constraints, path constraints, and control constraints are written directly as:

$$\boldsymbol{X}(-1) = \boldsymbol{X}_0, \quad \boldsymbol{\Phi}(\boldsymbol{X}(1)) = 0 \tag{7.62}$$

$$\boldsymbol{X}_{\min} \leq \boldsymbol{X}(\tau_k) \leq \boldsymbol{X}_{\max} \tag{7.63}$$

$$\begin{aligned} -F_{\max} &\leq \boldsymbol{u}(\tau_k)_1 \leq F_{\max} \\ -F_{\max} &\leq \boldsymbol{u}(\tau_k)_2 \leq F_{\max} \\ -a_{\text{tmax}} &\leq \boldsymbol{u}(\tau_k)_3 \leq 0 \end{aligned} \tag{7.64}$$

The energy optimal performance index J_g is discretized as:

$$J_g = \frac{t_f - t_0}{2} \int_{-1}^{1} \boldsymbol{u_g}^{\mathrm{T}}(\tau)\boldsymbol{u_g}(\tau)d\tau = \frac{t_f - t_0}{2} \sum_{k=1}^{M} \boldsymbol{U}^{\mathrm{T}}(\tau_k)\boldsymbol{U}(\tau_k)\omega_k \tag{7.65}$$

Therefore the object function in Eq. (7.65) and the various constraints in Eqs. (7.58), (7.61)–(7.64) finally formulate the original continuous optimization problem as an NLP. The optimized state variables $\boldsymbol{X}(\tau_i)$, $i = 0, 1, 2, \ldots, M$ and the control force $\boldsymbol{U}(\tau_k)$, $k = 1, 2, \ldots, M$. These

parameters can be solved by SNOPT optimization algorithm and corresponding software [19]. And the optimal discrete control force $\boldsymbol{U}(\tau_k)$ and optimal discrete trajectory $\boldsymbol{X}(\tau_i)$ are obtained. The continuous optimal control force and trajectory is obtained via the Lagrange interpolation towards discrete points.

7.2.2 Coupled Coordinated Control Method

7.2.2.1 Thrusters Layout of Operation Robot

The operation robot is assumed to be a $l_1 \times l_2 \times l_3$ cubic body. The thrusters layout is shown in Fig. 7.3. The thruster f_1 is equipped in a positive $o_c x_c$ axis, and the thruster f_2 is equipped in a negative $o_c x_c$ axis. The thruster f_3 is equipped in positive $o_c y_c$ axis, and the thruster f_4 is equipped in a negative $o_c y_c$ axis. The thruster f_5 is equipped in a positive $o_c z_c$ axis, and the thruster f_6 is equipped in a negative $o_c z_c$ axis. If this thruster layout is adopted, the input matrix of the thrusters layout $\boldsymbol{C}_r$ can be expressed by:

$$\boldsymbol{C}_r = \begin{bmatrix} 1 & -1 & 0 & 0 & 0 & 0 \\ 0 & 0 & 1 & -1 & 0 & 0 \\ 0 & 0 & 0 & 0 & 1 & -1 \\ 0 & 0 & \frac{l_3}{2} & \frac{l_3}{2} & \frac{l_2}{2} & \frac{l_2}{2} \\ -\frac{l_3}{2} & -\frac{l_3}{2} & 0 & 0 & -\frac{l_1}{2} & -\frac{l_1}{2} \\ \frac{l_2}{2} & \frac{l_2}{2} & \frac{l_1}{2} & \frac{l_1}{2} & 0 & 0 \end{bmatrix} \tag{7.66}$$

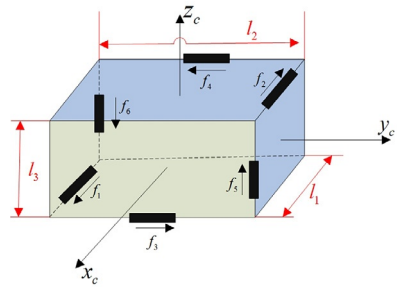

Fig. 7.3 Thrusters layout and simplified dimension of operation robot.

7.2.2.2 Coupled Coordinated Controller Design

The coupled dynamics model of the TSR is shown as Eqs. (7.42)–(7.48). We can see the law of the tether length is decoupled with the attitude movement. Therefore the releasing motor can control the length of the space tether solely, which can not influence on the attitude. The in-plane angle α, out-of-plane angle β, and the attitude angles are controlled by the thrusters of the operation robot.

It is defined that $\boldsymbol{u}' = [u_1 \;\; u_2 \;\; 0 \;\; M_x \;\; M_y \;\; M_z]^{\mathrm{T}}$ are the thruster control vectors in the tether coordinate frame $o_s x_2 y_2 z_2$ if we do not consider tether length in this controller. It is assumed that the thruster force vector is $\boldsymbol{u}_{\mathrm{T}} = [f_1 \;\; f_2 \;\; f_3 \;\; f_4 \;\; f_5 \;\; f_6]^{\mathrm{T}}$ in the body coordinate frame $o_c x_c y_c z_c$. The following relationship can be obtained:

$$\boldsymbol{u}' = \begin{bmatrix} {}^{b}\boldsymbol{C}_l^T & \boldsymbol{0} \\ \boldsymbol{0} & \mathbf{I}_{3\times 3} \end{bmatrix} \boldsymbol{C}_r \boldsymbol{u}_{\mathrm{T}} \tag{7.67}$$

where ${}^{b}\boldsymbol{C}_l$ is the transformed matrix from the coordinate frame $o_s x_2 y_2 z_2$ to $o_c x_c y_c z_c$.

The 6-DOF coupled coordinated controller contains two parts: a 6-DOF sliding mode controller and a PD controller for releasing the space tether. The thruster control force can be obtained through the 6-DOF sliding mode controller. The tether length can be controlled by the PD controller. The overall control diagram of coordinated control method is shown in Fig. 7.4.

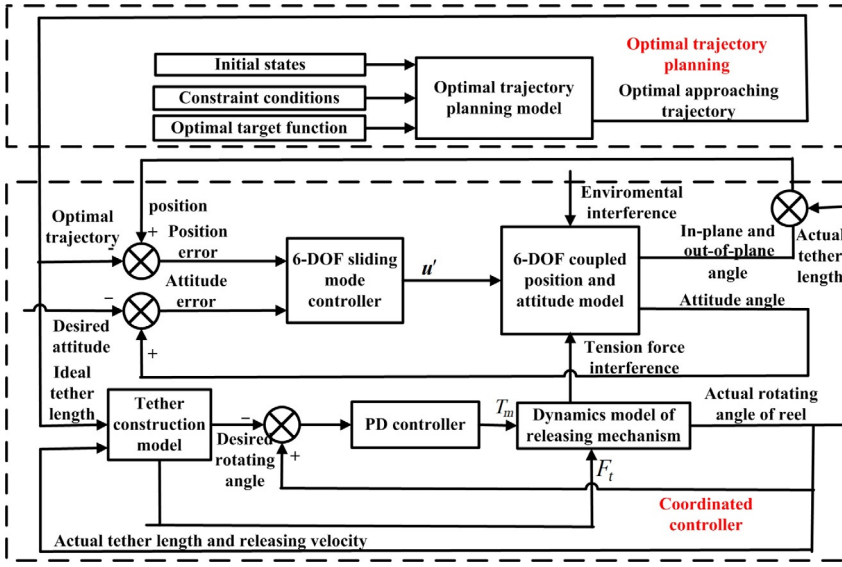

Fig. 7.4 Overall control diagram of coordinated control method.

Firstly, the 6-DOF sliding mode controller is introduced. The thruster active control vector $\boldsymbol{u}_s = [u_{s1} \;\; u_{s2} \;\; u_{s3} \;\; M_{sx} \;\; M_{sy} \;\; M_{sz}]^{\mathrm{T}}$ is obtained directly by the 6-DOF sliding mode controller. Then the control vector $\boldsymbol{u}'$ is obtained through $\boldsymbol{u}_s$: $u_1 = u_{s1}$, $u_2 = u_{s2}$, $M_x = M_{sx}$, $M_y = M_{sy}$, and $M_z = M_{sz}$. The six thruster control force vector $\boldsymbol{u}_{\mathrm{T}}$ can be calculated by Eq. (7.67).

Defined: $x_1 = \alpha$, $x_2 = \dot{\alpha}$, $x_3 = \beta$, $x_4 = \dot{\beta}$, $x_5 = l$, $x_6 = \dot{l}$, $x_7 = \phi_l$, $x_8 = \dot{\phi}_l$, $x_9 = \theta_l$, $x_{10} = \dot{\theta}_l$, $x_{11} = \psi_l$, and $x_{12} = \dot{\psi}_l$. The state vector of the 6-DOF coupled dynamics model can be rewritten as:

$$\dot{x}_1 = x_2 \tag{7.68}$$

$$\dot{x}_2 = -2(x_2 - \Omega_r)\left(\frac{x_6}{x_5} - x_4 \tan x_3\right) - 3\Omega_r^2 \sin x_1 \cos x_1 + \frac{u_{s1}}{\cos(x_3) x_5 m_r} \tag{7.69}$$

$$\dot{x}_3 = x_4 \tag{7.70}$$

$$\dot{x}_4 = -2\frac{x_6}{x_5}x_4 - \left[(x_2 - \Omega_r)^2 + 3\Omega_r^2 \cos^2 x_1\right] \sin x_3 \cos x_3 - \frac{u_{s2}}{x_5 m_r} \tag{7.71}$$

$$\dot{x}_5 = x_6 \tag{7.72}$$

$$\dot{x}_6 = u_{s3} \tag{7.73}$$

$$\dot{x}_7 = x_8 \tag{7.74}$$

$$\begin{aligned} \dot{x}_8 = {} & n_x \Omega_r^2 \left(\sin^2 x_3 - \cos^2 x_3\right) x_7 + (n_x + 1)\Omega_r \sin x_3 x_{10} \\ & + (1 - n_x)\Omega_r \cos x_3 x_{12} + \Omega_r \cos x_3 x_4 x_9 \\ & - \Omega_r \sin x_3 x_4 x_{11} - n_x \Omega_r^2 \sin x_3 \cos x_3 + \frac{M_{sx}}{I_x} \end{aligned} \tag{7.75}$$

$$\dot{x}_9 = x_{10} \tag{7.76}$$

$$\begin{aligned} \dot{x}_{10} = {} & n_y \Omega_r \sin x_3 x_9 - \left(\sin x_3 - n_y \sin x_3\right) \Omega_r x_8 \\ & - \Omega_r \cos x_3 x_4 x_7 + n_y \Omega_r^2 \sin x_3 \cos x_3 x_{11} - \Omega_r \sin x_3 x_4 + \frac{M_{sy}}{I_y} \end{aligned} \tag{7.77}$$

$$\dot{x}_{11} = x_{12} \tag{7.78}$$

$$\begin{aligned} \dot{x}_{12} = {} & -n_z \Omega_r^2 \cos^2 x_3 x_{11} + (n_z - 1)\Omega_r \cos x_3 x_8 + \Omega_r \sin x_3 x_4 x_7 \\ & - n_z \Omega_r^2 \sin x_3 \cos x_3 x_9 - \Omega_r \cos x_3 x_4 + \frac{M_{sz}}{I_z} \end{aligned} \tag{7.79}$$

Eqs. (7.68)–(7.79) can be simplified and expressed as:

$$\dot{\boldsymbol{x}} = f(\boldsymbol{x}, \dot{\boldsymbol{x}}, t) + \boldsymbol{D} + \boldsymbol{u}_s \tag{7.80}$$

where $\boldsymbol{D}$ denotes all kinds of interference (i.e., environmental interference and tension force disturbed torque), $\boldsymbol{x}$ is the states vector. Now, the sliding mode controller is designed. We defined the state error $\boldsymbol{e} = \boldsymbol{x} - \boldsymbol{x}_q$, where $\boldsymbol{x}_q$ is the desired states of operation robot. Therefore:

$$\begin{aligned} \dot{\boldsymbol{e}} &= \dot{\boldsymbol{x}} - \dot{\boldsymbol{x}}_q \\ \ddot{\boldsymbol{e}} &= \ddot{\boldsymbol{x}} - \ddot{\boldsymbol{x}}_q \end{aligned} \tag{7.81}$$

The switch function is chosen as:

$$\boldsymbol{S} = \boldsymbol{e} + \boldsymbol{\Lambda e} \tag{7.82}$$

where $\boldsymbol{\Lambda}$ is 6×6 unit matrix. If the system lies in a sliding mode $\boldsymbol{S} = \boldsymbol{0}$, the system is stable. The index approach law is designed to make the system change into $\boldsymbol{S} = \boldsymbol{0}$ from the nonsliding mode state.

$$\dot{\boldsymbol{S}} = -\boldsymbol{K}\boldsymbol{S} - \boldsymbol{\varepsilon}\,\mathrm{sgn}(\boldsymbol{S}) \tag{7.83}$$

where $\boldsymbol{K} = \mathrm{diag}(k_1 \ldots k_6)$, $\boldsymbol{\varepsilon} = \mathrm{diag}(\varepsilon_1 \ldots \varepsilon_6)$, $k_i,\ \varepsilon_i > 0$, $\mathrm{sgn}(\boldsymbol{S}) = [\,\mathrm{sgn}(s_1) \ldots \mathrm{sgn}(s_6)]^{\mathrm{T}}$. The index approach equation is $-\boldsymbol{K}\boldsymbol{S}$ and the equal approach equation $-\boldsymbol{\varepsilon}\,\mathrm{sgn}(\boldsymbol{S})$.

The switch function (Eq. 7.82) is differentiated and substituted into Eq. (7.83):

$$\ddot{\boldsymbol{x}} - \ddot{\boldsymbol{x}}_{\boldsymbol{q}} + \boldsymbol{\Lambda}\dot{\boldsymbol{e}} = -\boldsymbol{K}\boldsymbol{S} - \boldsymbol{\varepsilon}\,\mathrm{sgn}(\boldsymbol{S}) \tag{7.84}$$

Substituted Eq. (7.80) into (7.84):

$$f(\boldsymbol{x}, \boldsymbol{x}, t) + \boldsymbol{D} + \boldsymbol{u}_s = \ddot{\boldsymbol{x}}_{\boldsymbol{q}} - \boldsymbol{\Lambda}\dot{\boldsymbol{e}} - \boldsymbol{K}\boldsymbol{S} - \boldsymbol{\varepsilon}\,\mathrm{sgn}(\boldsymbol{S}) \tag{7.85}$$

Therefore the sliding mode control law is obtained by Eq. (7.85):

$$\boldsymbol{u}_s = -f(\boldsymbol{x}, \boldsymbol{x}, t) - \boldsymbol{D} + \ddot{\boldsymbol{x}}_{\boldsymbol{q}} - (\boldsymbol{\Lambda} + \boldsymbol{K})\dot{\boldsymbol{e}} - \boldsymbol{K}\boldsymbol{\Lambda}\boldsymbol{e} - \boldsymbol{\varepsilon}\,\mathrm{sgn}(\boldsymbol{S}) \tag{7.86}$$

where $\boldsymbol{D}$ is unknown. However, $\boldsymbol{D}$ is bounded. If the upper bound $\boldsymbol{D}_h$ is estimated, the control law is rewritten as:

$$\boldsymbol{u}_s = -f(\boldsymbol{x}, \boldsymbol{x}, t) - \boldsymbol{D}_h\,\mathrm{sgn}(\boldsymbol{S}) + \ddot{\boldsymbol{x}}_{\boldsymbol{q}} - (\boldsymbol{\Lambda} + \boldsymbol{K})\dot{\boldsymbol{e}} - \boldsymbol{K}\boldsymbol{\Lambda}\boldsymbol{e} - \boldsymbol{\varepsilon}\,\mathrm{sgn}(\boldsymbol{S}) \tag{7.87}$$

The tension force of the space tether F_t can be estimated by Eq. (7.31). The interferential torque is related to the tension force and the connection point between the tether and operation robot. Define the distance between the connection point and the centroid of the operation robot as l_x, l_y, and l_z in the body frame. The interferential torque $\boldsymbol{T}_t$ can be estimated by Eq. (7.88).

$$\boldsymbol{T}_t = \boldsymbol{l}^{\times b}\boldsymbol{C}_l[0 \quad 0 \quad -F_t]^{\mathrm{T}} \tag{7.88}$$

Secondly, the PD controller for releasing the space tether is provided. The control torque of releasing the reel can supply negative acceleration, which can control the tether length associated with initial velocity of the operation robot. The ideal releasing length of the space tether can be obtained by the optimal trajectory planning model. The desired rotating angle ϕ_{rq} and angular velocity $\dot{\phi}_{rq}$ are obtained by Eq. (7.40). If we define the actual rotating angle of the reel is ϕ_r, and the corresponding angular velocity is $\dot{\phi}_r$, the PD control law is provided as:

$$T_m = K_p\left(\phi_r - \phi_{rq}\right) + K_d\left(\dot{\phi}_r - \dot{\phi}_{rq}\right) \tag{7.89}$$

where K_p and K_d denote the proportion and differential coefficients separately.

Define the Lyapunov function as follows:

$$V = \frac{1}{2}\boldsymbol{S}^{\mathrm{T}}\boldsymbol{S} \tag{7.90}$$

The differentiating Eq. (7.90) yields:

$$\dot{V} = \boldsymbol{S}^{\mathrm{T}}\dot{\boldsymbol{S}} = \boldsymbol{S}^{\mathrm{T}}(\ddot{\boldsymbol{e}} + \boldsymbol{\Lambda}\dot{\boldsymbol{e}}) = \boldsymbol{S}^{\mathrm{T}}\left[f(\boldsymbol{x}, \boldsymbol{x}, t) + \boldsymbol{D} + \boldsymbol{u}_s - \ddot{\boldsymbol{x}}_{\boldsymbol{q}} + \boldsymbol{\Lambda}\dot{\boldsymbol{e}}\right] \tag{7.91}$$

Substitute Eq. (7.87) into (7.91):

$$\dot{V} = \boldsymbol{S}^{\mathrm{T}}(\ddot{\boldsymbol{e}} + \boldsymbol{\Lambda}\dot{\boldsymbol{e}}) = \boldsymbol{S}^{\mathrm{T}}\left[-\boldsymbol{K}\boldsymbol{S} - \boldsymbol{\varepsilon}\,\mathrm{sgn}(\boldsymbol{S}) + \boldsymbol{D} - \boldsymbol{D}_h\,\mathrm{sgn}(\boldsymbol{S})\right] \le -\boldsymbol{S}^{\mathrm{T}}\boldsymbol{K}\boldsymbol{S} \le 0 \tag{7.92}$$

The 6-DOF sliding mode controller has the characteristics of global stability from Eq. (7.92) and the Lyapunov stability theory.

The stability of the PD controller for releasing the tether is decided by K_p and K_d. Therefore the proper K_p and K_d should be selected according to the engineering experience.

7.3 NUMERICAL SIMULATION

Assume: The target and space platform move in the same circular orbit. The operation robot is approximately 50 kg and the space platform is about 2000kg. The initial length of the space tether l_0 is 0.01 m. The initial velocity of the operation robot $\dot{l}_0$ is 2 m/s. The initial in-plane angle α_0 is $\frac{\pi}{4}$rad. The initial out-of-plane angle β_0 is 0 rad. The parameters of the operation robot are $l_1 = l_2 = l_3 = 0.8$ m. The position parameters of the connection point are $l_x = l_y = 0$ m, $l_z = -0.4$ m. It is assumed that the control force error of the

thruster is $F \pm 0.02F$ (F is the desired control force). The initial attitude angles are $\phi_{l0} = \theta_{l0} = \psi_{l0} = \dfrac{\pi}{12}$ rad, and the desired attitude angles are $\phi_{lq} = \theta_{lq} = \psi_{lq} = 0$ rad.

$$I = \begin{bmatrix} 8 & -0.0025 & -0.00032 \\ -0.0025 & 8 & -0.00086 \\ -0.00032 & -0.00086 & 8 \end{bmatrix} \text{kg m}^2,$$

$$\Lambda = \text{diag}(0.03, 0.03, 0.03, 0.2, 0.2, 0.2),$$

$$K = \text{diag}(0.1, 0.1, 0.1, 0.5, 0.5, 0.5),$$

$$\varepsilon = \text{diag}(0.00001, 0.00001, 0.00001, 0.00001, 0.00001, 0.00001).$$

The maximum thruster force is 1.5 N. The environmental interference are:

$$\boldsymbol{D}_1 = \begin{cases} \sin(\Omega_r t) \times 10^{-3} \text{ N} \\ 1.2\sin(\Omega_r t) \times 10^{-3} \text{ N} \\ 1.1\sin(\Omega_r t) \times 10^{-3} \text{ N} \\ [3\cos(\Omega_r t) + 1] \times 10^{-5} \text{ N m} \\ [1.5\sin(\Omega_r t) + 3\cos(\Omega_r t)] \times 10^{-5} \text{ N m} \\ [3\sin(\Omega_r t) + 1] \times 10^{-5} \text{ N m} \end{cases}$$

and its upper bound are:

$$\boldsymbol{D}_h = \begin{cases} 0.0015 + 0.05 \text{ N} \\ 0.0015 + 0.05 \text{ N} \\ 0.0015 + 0.1 \text{ N} \\ 0.00004 + 0.001 \text{ N m} \\ 0.00005 + 0.001 \text{ N m} \\ 0.00004 + 0.001 \text{ N m} \end{cases}$$

The rest of the parameters are shown in Table 7.1.

Fig. 7.5 shows the releasing trajectory of the operation robot in the orbital frame $o_S x_S y_S z_S$. Fig. 7.6 shows the relative trajectory comparison of the operation robot in the target orbital frame. From the simulation results, we can see that the optimal trajectory seems smooth, which the operation robot can track it easily, and the operation robot can approach the

Table 7.1 Simulation parameters

The orbital parameters of target satellite	The orbital parameters of space platform	Control parameters	The parameters of releasing mechanism
Orbit altitude: 622 km Argument of perigee: 20 degrees Longitude ascending node: 0 degree Orbit inclination: 10 degrees Eccentricity: 0 degree		$K_p = 0.1$ $K_d = 0.1$	$EA = 25997$ N, $\gamma = 1$ $w_d = 0.06$ m, $d = 0.03$ mm $L_t = 300$ m, $D_1 = 0.04$ m $C_t = 0.02$, $I_r = 7.72e-5$ kg m^2 $C_d = 2e-6$, $T_l = 0.00034$ N m
True anomaly: 0.002 degrees	True anomaly: 0 degree		

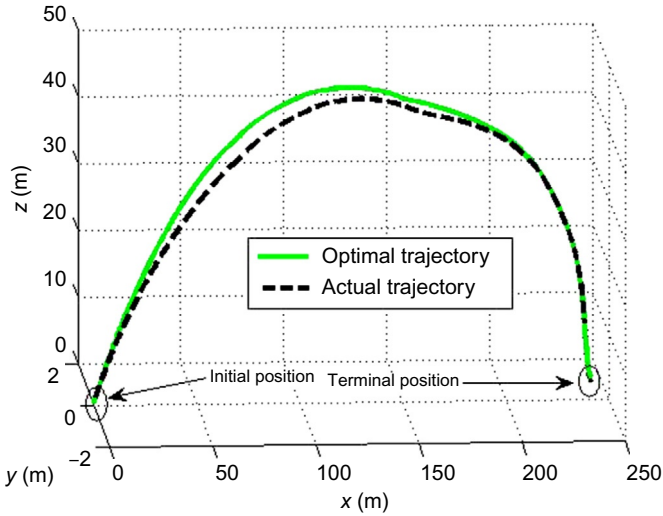

Fig. 7.5 Releasing trajectory of operation robot.

target for tracking the optimal trajectory using the coupled coordinated control method. Although the operation robot may deviate from the optimal trajectory, the terminal accuracy is kept within ±0.1 m. The in-plane angle of the operation robot is provided in Fig. 7.7, and the out-of-plane angle is provided in Fig. 7.8. There is deviation between 0 and 150 s. However, the operation robot can track the desired in-plane and out-of-plane angles accurately after 150 s. Fig. 7.9 shows the releasing length of the space tether. It is concluded that the changing trend of the tether's actual length is similar with the desired length trend, which illustrates that the control accuracy of the

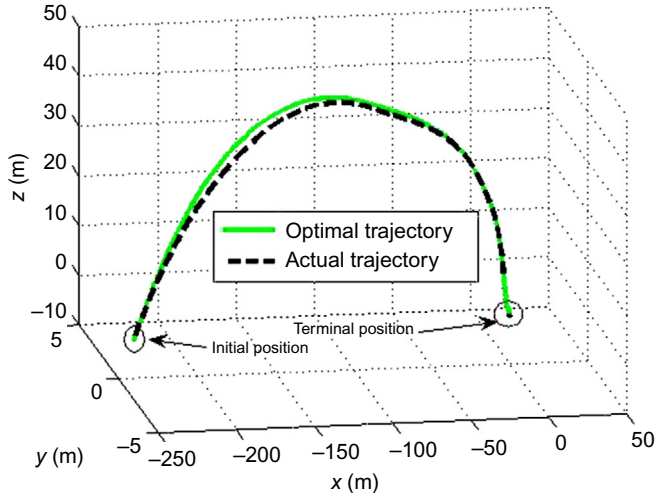

Fig. 7.6 Relative trajectory of operation robot.

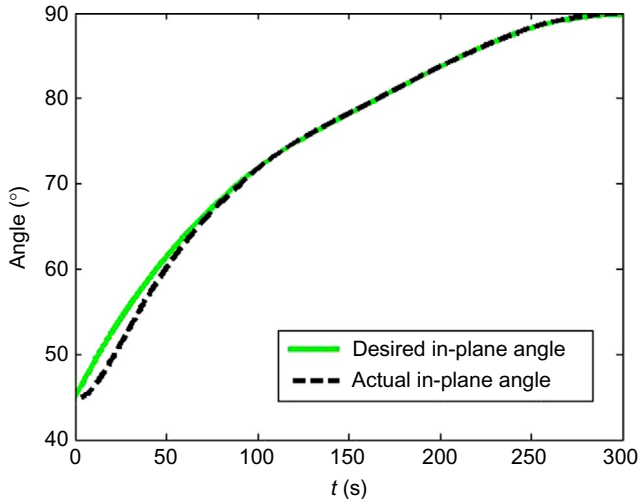

Fig. 7.7 In-plane angle of operation robot.

releasing mechanism is well. Fig. 7.10 shows the releasing velocity comparison of the space tether. The releasing velocity is kept unchanged or reduced, which satisfies the rule of the releasing characteristics of the space tether.

Figs. 7.11 and 7.12 show the rotating angle and the rotating angular velocity of the reel. The releasing reel can rotate continuously between 0 and 250 s, which illustrates that the tether can be released by the reel in

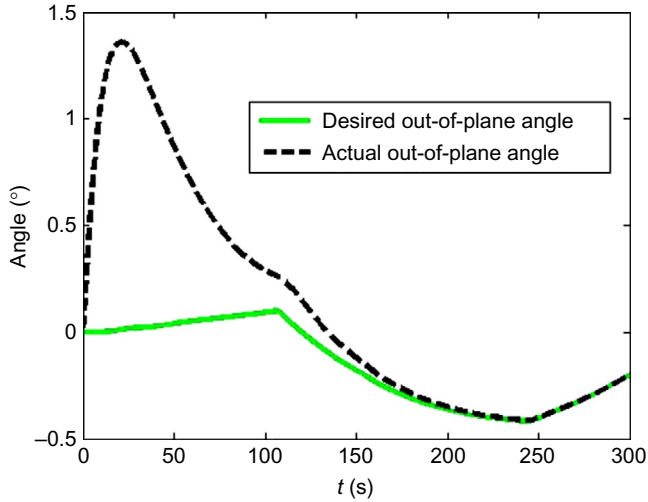

Fig. 7.8 Out-of-plane angle of operation robot.

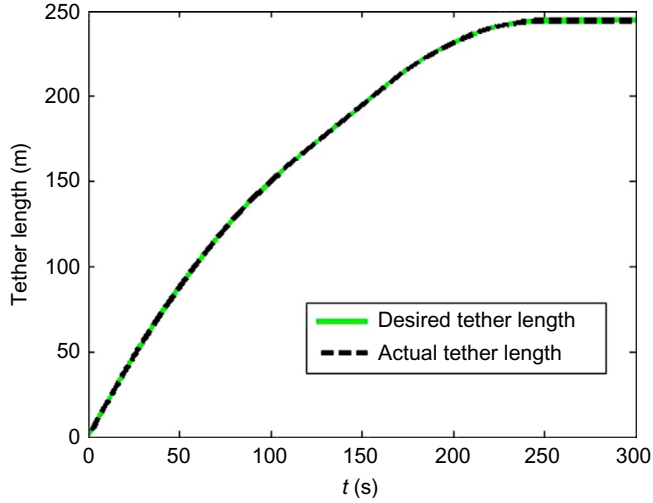

Fig. 7.9 Releasing length of space tether.

this period. From 250 to 300 s, the releasing reel cannot rotate, because the tether has been stopped, and the operation robot tracks the optimal trajectory through changing the in-plane and out-of-plane angle.

Figs. 7.13 and 7.14 show the attitude angle and the attitude angular velocity of the operation robot. The desired attitude angle is 0 degree, and the initial attitude angle is 15 degrees. The yaw, pitch, and roll angles

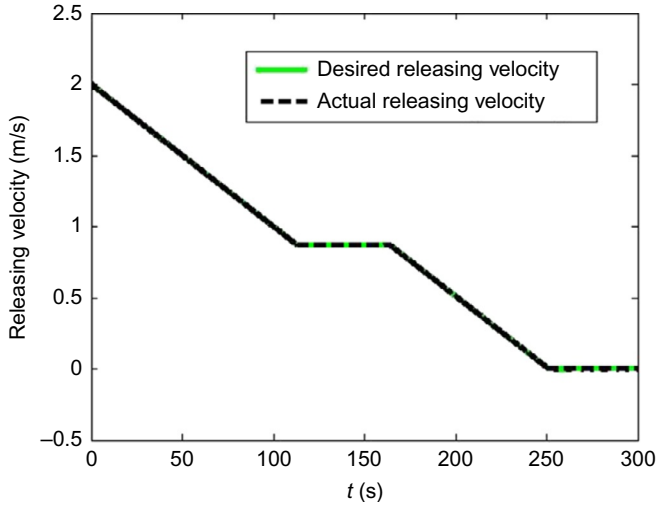

Fig. 7.10 Releasing velocity of space tether.

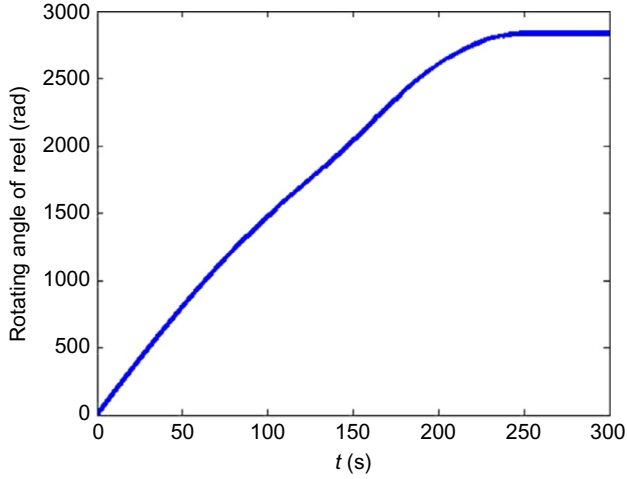

Fig. 7.11 Rotating angle of reel.

can change to the desired attitude angle 0 degree using the coordinated coupled control method. And all the angles are kept in ±0.3 degrees. The angular velocity of the operation robot is kept ±0.02 degrees/s after 50 s, which satisfies attitude control requirements.

Figs. 7.15 and 7.16 show the attitude control torque of the coupled coordinated control method and the angular velocity of the operation robot.

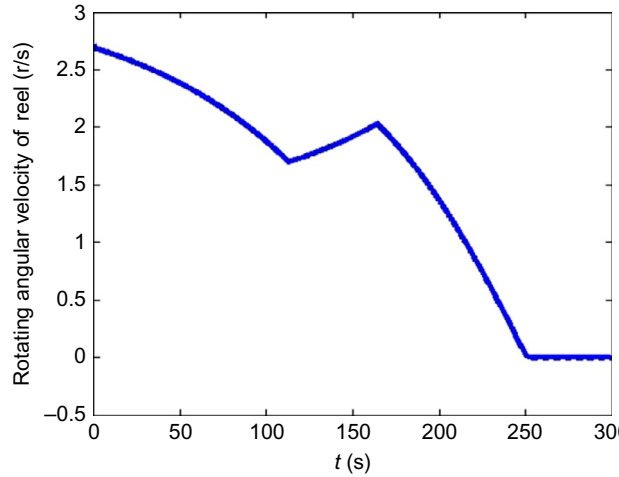

Fig. 7.12 Rotating angular velocity of reel.

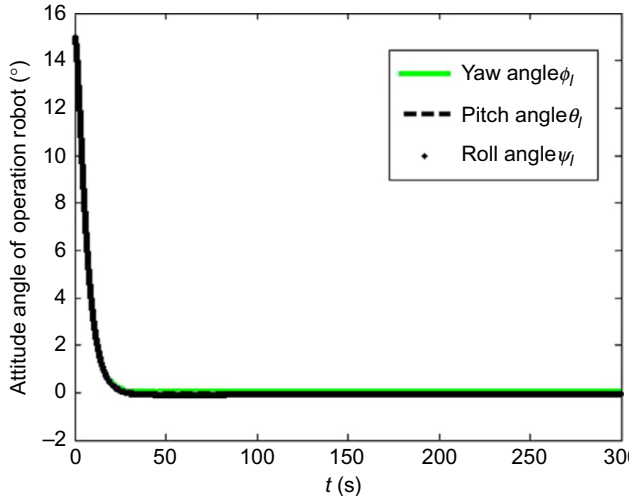

Fig. 7.13 Attitude angle of operation robot.

The attitude control torque is kept within ± 0.25 m in the period of 0–30 s. In this period, the attitude angle become the desired angle 0 degree. The angular velocity of the operation robot in the x- and z-directions is controlled to be 0 degree/s after 50 s, and the angular velocity in y-direction is kept about -0.6 degrees/s. This is because the angular velocity describes the composite motion of tether motion and orbital motion of space platform.

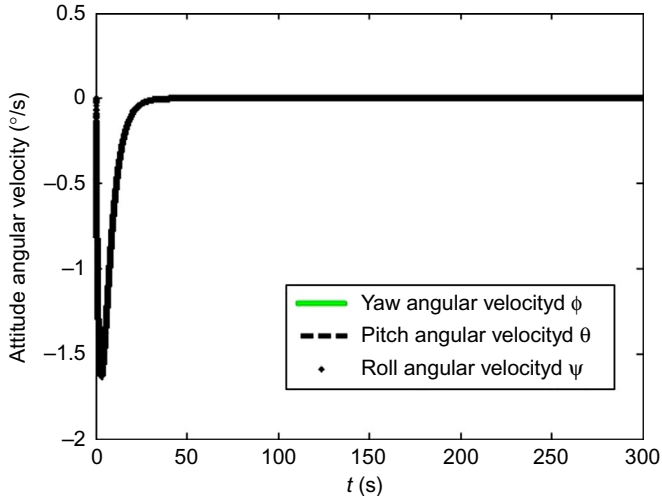

Fig. 7.14 Attitude angular velocity.

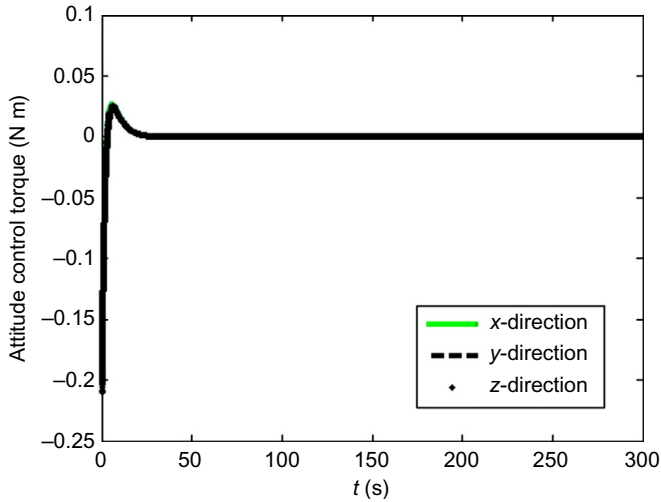

Fig. 7.15 Attitude control torque.

Figs. 7.17 and 7.18 show the tension force and the attitude interference torque of the space tether. It can be seen that the tension force of the tether is kept 0.15 N between 0 and 15 s, and the tension force is small after 15 s. This is because the reel lies in an unstable state before 15 s, and the reel rotates steadily after 15 s. The tether tension force can lead to attitude interferential

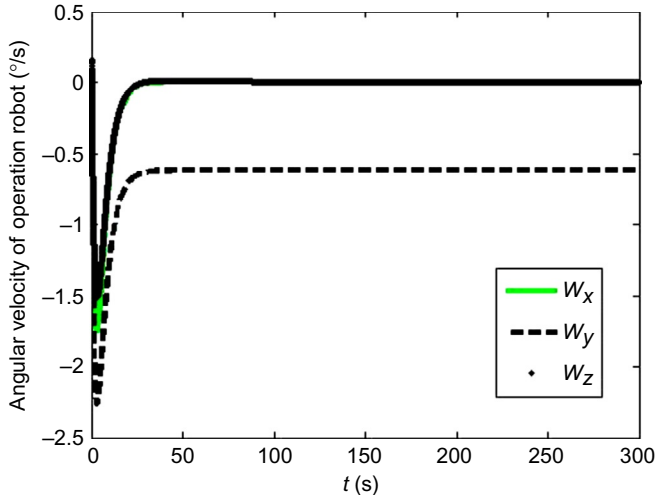

Fig. 7.16 Angular velocity of operation robot.

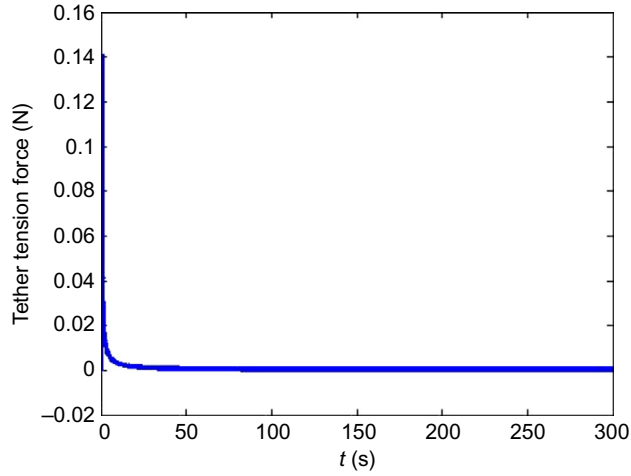

Fig. 7.17 Tension force of space tether.

torque, because the overlapping between the centroid of the operation robot and the connection point is difficult. In the early period, there is a relative large disturbed attitude torque, which can reflect the phenomenon in Fig. 7.17. The control torque of the releasing motor is shown in Fig. 7.19. In the period between 0 and 15 s, the control torque of the reel is kept about 0.02 N m. The control torque fluctuates in ±2 mN m.

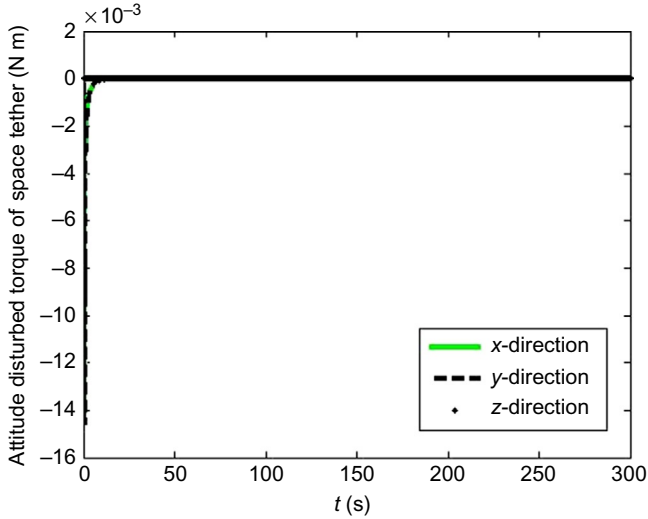

Fig. 7.18 Attitude interference torque of tether.

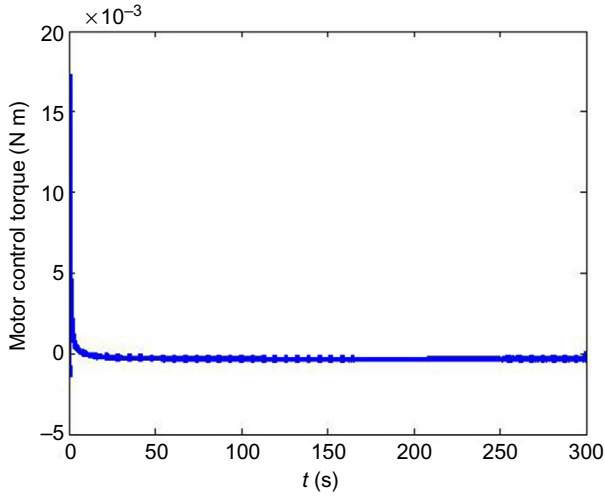

Fig. 7.19 Control torque of releasing motor.

Fig. 7.20 shows the control force in the tether coordinate frame. The control force in the x-direction is kept within ± 2.5 N between 0 and 50 s, and ± 0.5 N after 50 s. And the control force in they-direction is kept within ± 0.5 N all the control period. Figs. 7.21–7.26 represent the thruster

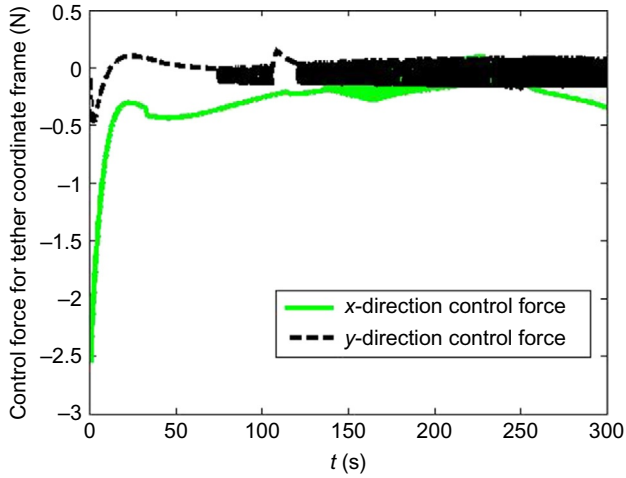

Fig. 7.20 Control force in tether coordinate frame.

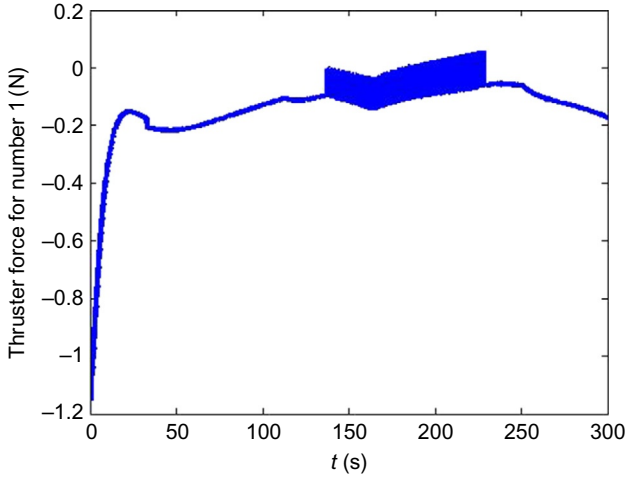

Fig. 7.21 Force of thruster 1.

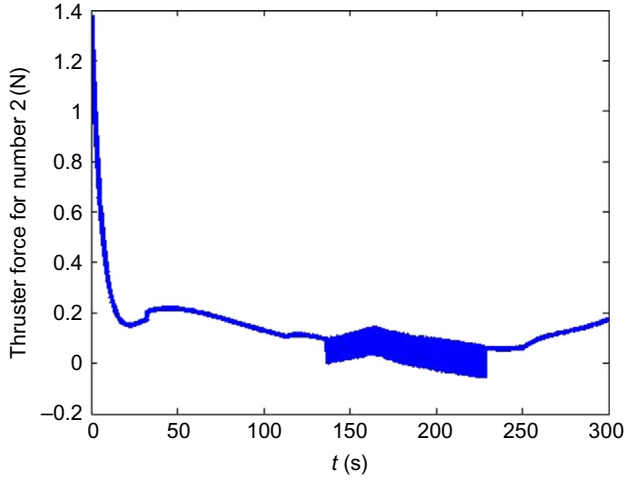

Fig. 7.22 Force of thruster 2.

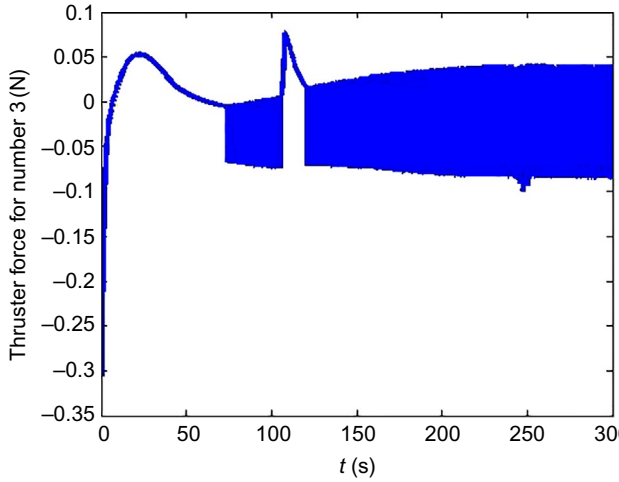

Fig. 7.23 Force of thruster 3.

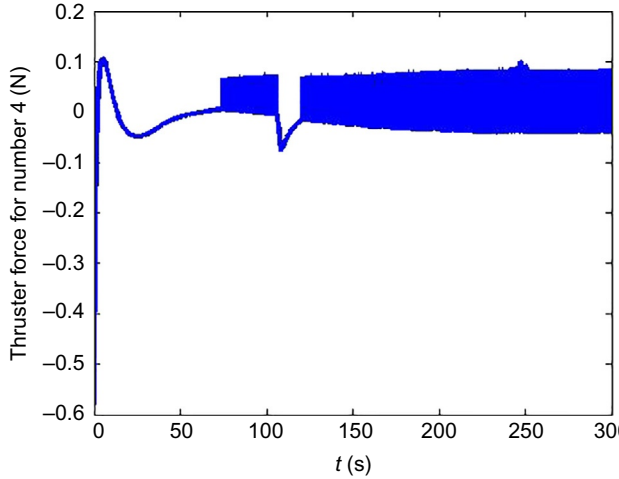

Fig. 7.24 Force of thruster 4.

force in numbers 1–6. We can see the control force of thruster 1 is kept within ±1.2 N, the control force of thruster 2 ±1.4 N, the control force of thruster 3 ±0.35 N, the control force of thruster 4 and 6 ±0.6 N, and the control force of thruster 5 ±0.25 N. Therefore all the forces of these thrusters are under 1.5 N, which satisfies the requirement of the maximum thruster force. The operation robot can track the optimal trajectory and desired attitude angles for the control of six thrusters and the releasing reel.

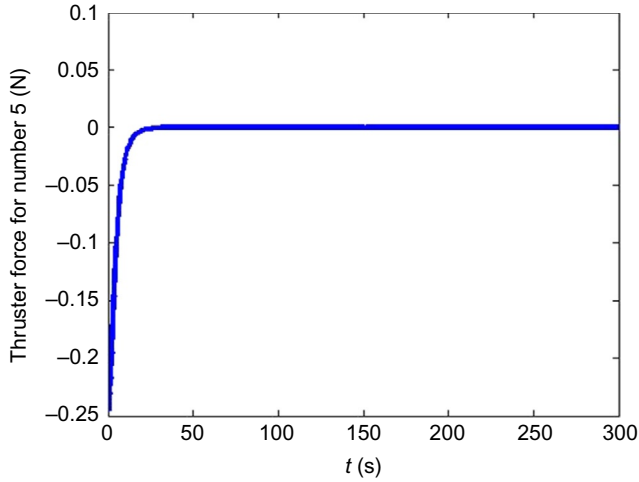

Fig. 7.25 Force of thruster 5.

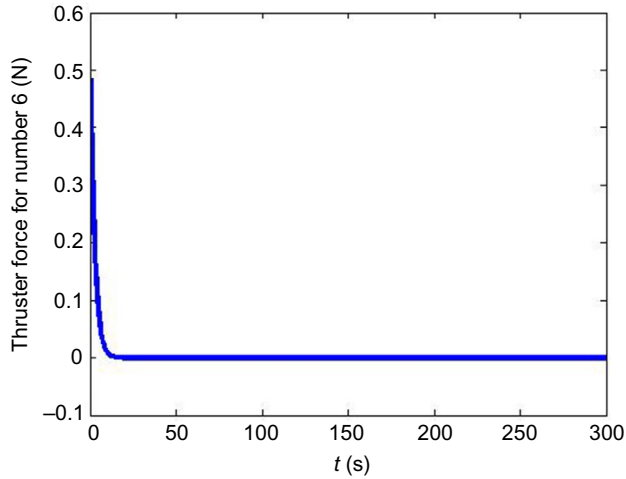

Fig. 7.26 Force of thruster 6.

REFERENCES

[1] Y. Ulybyshev, Trajectory optimization for spacecraft proximity operations with constraints, in: AIAA Guidance, Navigation, and Control Conference, Portland, Oregon, 2011.

[2] Y. Ulybyshev, Spacecraft trajectory optimization based on discrete sets of pseudo-impulses, in: AIAA/AAS Astrodynamics Specialist Conference and Exhibit, Honolulu, Hawaii, 2008.

[3] S. Suzuki, T. Yoshizawa, Multi-objective trajectory optimization by goal programming with fuzzy decisions, J. Guid. Control. Dyn. 17 (2) (1994) 297–303.
[4] E.V. Kampen, Q.P. Chu, J.A. Mulder, Optimization of spacecraft rendezvous and docking using interval analysis, in: AIAA Guidance, Navigation, and Control Conference, Toronto, Ontario, Canada, 2010.
[5] D.A. Benson, Gauss Pseudospectral Transcription for Optimal Control (Ph.D. thesis), Department of Aeronautics and Astronautics, Massachusetts Institute of Technology, USA, 2004.
[6] F. Fahroo, I.M. Ross, On discrete-time optimality conditions for pseudospectral methods, in: AIAA/AAS Astrodynamics Specialist Conference and Exhibit, Keystone, CO, 2006.
[7] T.D. Guo, F.H. Jiang, J.F. Li, Homotopic approach and pseudospectral method applied jointly to low thrust trajectory optimization, Acta Astronaut. 71 (2012) 38–50.
[8] D. Garg, M. Patterson, W.H. William, et al., A unified framework for the numerical solution of optimal control problems using pseudospectral methods, Automatica 46 (2010) 1843–1851.
[9] N. Yuya, S. Fumiki, N. Shinichi, Guidance control of "tethered retriever" with collaborative tension-thruster control for future on-orbit service missions, in: The 8th International Symposium On Artificial Intelligence: Robotics And Automation in Space-ISAIRAS, Munich, Germany, 2005.
[10] N. Masahiro, Attitude control of a tethered space robot by link motion under microgravity, in: Proceedings of the IEEE International Conference On Control Applications, 2004, Taipei, Taiwan, 2004.
[11] N. Masahiro, D.N. Nenchev, U. Masaru, Tethered robot casting using a spacecraft-mounted manipulator, J. Guid. Control. Dyn. 24 (4) (2001) 827–833.
[12] M. Osamu, M. Saburo, Collaborative control of tethered satellite cluster systems, in: AIAA Guidance, Navigation, and Control Conference and Exhibit, Montreal, Canada, 2001.
[13] Godard, K.D. Kumar, B. Tan, Fault-tolerant stabilization of a tethered satellite system using offset control, J. Spacecr. Rocket. 45 (5) (2008) 1070–1084.
[14] M. Kruijff, E.J. van der Heide, YES2, the second young engineers satellite a tethered inherently-safe re-entry capsule, in: 53th International Astronautical Congress of the International Astronautical Federation, Houston, October 10–19, 2002.
[15] C. Menon, M. Kruijff, A. Vavouliotis, Design and testing of a space mechanism for tether deployment, J. Spacecr. Rocket. 44 (4) (2007) 927–939.
[16] J.A. Carroll, SEDS deployer design and flight performance, in: AIAA Space Programs and Technologies Conference and Exhibit, Huntsville, September 21–23, 1993.
[17] Y. Nakamura, H. Hashimoto, Ground test of tether deployment and retrieval along optimal path with a tether reeling mechanism designed for micro-class satellites, in: 54th International Astronautical Congress of the International Astronautical Federation, Bremen, Germany, September 29–October 3, 2003.
[18] Y. Sakamoto, T. Yasaka, Study of low-cost orbit determination system for tethered satellites, J. Space Technol. Sci. 16 (1) (2002) 1–10.
[19] P.E. Gill, W. Murray, M.A. Saunders, SNOPT: an SQP algorithm for large-scale constrained optimization, SIAM J. Optim. 12 (2002) 979–1006.